Thermochimica Acta 506 (2010) 20–27

Contents lists available at ScienceDirect

Thermochimica Acta

journal homepage: www.elsevier.com/locate/tca

Thermodynamic modeling, structural and spectroscopic studies of the $KNbWO_6$–$KSbWO_6$–$KTaWO_6$ system

Aleksandr V. Knyazev[a,*], Miroslaw Mączka[b], Nataliya Yu. Kuznetsova[a]

[a] Nizhny Novgorod State University, Gagarin Prospekt 23/2, 603950 Nizhny Novgorod, Russia
[b] Institute of Low Temperature and Structure Research, Polish Academy of Sciences, P.O. Box 1410, 50-950 Wroclaw, Poland

ARTICLE INFO

Article history:
Received 11 March 2010
Received in revised form 6 April 2010
Accepted 7 April 2010
Available online 14 April 2010

Keywords:
Thermodynamic modeling
Defect pyrochlore
IR and Raman spectroscopy
X-ray diffraction
Isomorphism
Mixing diagram

ABSTRACT

In the present work some structural and thermodynamic features in $KNb_xSb_yTa_zWO_6$ solid-state solutions were investigated. A mathematical subregular ternary solutions model is advanced. The compounds have been structurally studied using X-ray diffraction. In particular, structure of individual compounds ($KNbWO_6$, $KSbWO_6$ and $KTaWO_6$) was refined by the Rietveld method (space group $Fd3m$, $Z=8$). IR and Raman spectroscopies were used to assign vibrational bands and determine structural pecularities. The differential scanning calorimetry was applied to measure decomposition temperature of compounds under study and to detect any possible phase transitions.

1. Introduction

Pyrochlore is important in nature as an ore mineral (Nb and Ta) and as a carrier of lanthanide and actinide (Th and U) elements in the Earth's crust. The structure type exhibits a range of useful properties for materials science applications including ionic conductivity (both cations and anions) [1,2], electrical conductivity, magnetic [3–6] and ferroelectric [7] properties. Besides materials on basis of KA^VWO_6 (A^V – Nb, Sb, Ta) compounds can be used as catalysts due to content of transition metals.

The object of our investigation is complex oxides containing potassium, tungsten and transition metals with oxidation number +5 and solid-state solution on their base. Despite the extensive interest in defect pyrochlore oxides, thermodynamic and physicochemical data are presented in bare number of publications. Therefore detailed investigations of these compounds are especially important.

The goals of this work include detailed structural, spectroscopic and thermal stability studies of individual phases (KA^VWO_6 (A^V – Nb, Sb, Ta)), as well as thermodynamic modeling of the $KNb_xSb_yTa_zWO_6$ system.

2. Experimental

2.1. Samples

$KNb_xSb_yTa_zWO_6$ solid solution was prepared by the solid-state reaction between WO_3, Nb_2O_5, Sb_2O_3, Ta_2O_5 and KNO_3. The synthesis was performed in a porcelain crucible, into which the reaction mixture with the corresponding atomic ratio $1K+1W+xNb+ySb+zTa$ was loaded. In order to find out the mixing temperatures, the process was realized in several stages with temperature rise of 25 K and holding the reaction mixture at every temperature during 50 h. This process was started at 973 K. The choice of initial temperature is determined by the purity of studied compounds with pyrochlore structure compared to additive products, which form at lower temperature. The phase individuality of the compounds was verified after every synthesis step by X-ray diffraction. The X-ray data and estimated impurity content (0.5–1 wt%) in the substances allowed us to conclude that every of the studied samples was composed of an individual crystalline compound. To prove the atomic ration $1K+1W+xNb+ySb+zTa$ the obtained samples were analyzed on a Shimadzu energy-dispersive roentgen fluorescent spectrometer EDX-900HS (from $_{11}Na$ to $_{92}U$) with sensitive detector without liquid nitrogen.

In the case when at a given temperature a sample was detected to be two-phase, i.e. its X-ray diffraction pattern was a superposition of X-ray diffraction patterns of two solid solutions, the temperature was further increased by 25 K. Thus we took value

* Corresponding author. Tel.: +7 831 465 62 06; fax: +7 831 434 50 56.
E-mail address: knav@uic.nnov.ru (A.V. Knyazev).

0040-6031/$ – see front matter © 2010 Elsevier B.V. All rights reserved.
doi:10.1016/j.tca.2010.04.009

Table 1
Structural parameters, experimental and theoretical miscibility data for the isovalent substitutional solid solution of composition $KNb_xSb_yTa_zWO_6$ (all data presented at T = 298 K).

x	y	z	a (Å)	$\Delta_{mix}V$ (Å^3)	T_{mix} (K)	$\Delta_{mix}H^\circ$ (calc.) (kJ/mol)	$\Delta_{mix}H$ (model.) (kJ/mol)	$\Delta\bar{H}_1$ (kJ/mol)	$\Delta\bar{H}_2$ (kJ/mol)	$\Delta\bar{H}_3$ (kJ/mol)	$\ln\gamma_1$	$\ln\gamma_2$	$\ln\gamma_3$
1	0	0	10.5001(1)	0	–	0	0	0	22.20	22.20	0	8.96	8.96
0	1	0	10.23671(7)	0	–	0	0	31.08	0	22.20	12.54	0	8.96
0	0	1	10.4695(1)	0	–	0	0	11.10	31.08	0	4.48	12.54	0
0.125	0.875	0	10.2365(7)	−10.6	1073	3.36	3.28	22.10	0.59	31.28	8.91	0.24	12.62
0.25	0.75	0	10.2651(14)	−12.4	1098	5.13	5.41	14.99	2.22	33.75	6.05	0.90	13.62
0.375	0.625	0	10.2934(9)	−14.0	1123	6.18	6.50	9.54	4.68	31.63	3.85	1.89	12.77
0.5	0.5	0	10.3627(34)	−2.4	1123	6.47	6.66	5.55	7.77	26.92	2.24	3.13	10.86
0.625	0.375	0	10.4255(5)	7.3	1098	6.04	5.98	2.81	11.27	21.61	1.13	4.55	8.72
0.75	0.25	0	10.4589(5)	7.7	1073	5.02	4.58	1.11	14.99	17.73	0.45	6.05	7.15
0.875	0.125	0	10.4768(16)	2.9	1023	3.20	2.55	0.24	18.70	17.25	0.10	7.54	6.96
0.125	0	0.875	10.4598(17)	−4.4	–	*1.76*	1.37	10.62	40.20	0.04	4.29	16.22	0.02
0.25	0	0.75	10.4659(9)	−3.7	–	*2.91*	2.60	9.37	41.87	0.35	3.78	16.89	0.14
0.375	0	0.625	10.4947(10)	4.5	–	*3.63*	3.58	7.59	38.35	1.17	3.06	15.47	0.47
0.5	0	0.5	10.4914(8)	2.2	–	*3.88*	4.16	5.55	31.91	2.78	2.24	12.87	1.12
0.625	0	0.375	10.4923(7)	1.2	–	*3.63*	4.23	3.51	24.81	5.42	1.42	10.01	2.19
0.75	0	0.25	10.4998(11)	2.5	–	*2.91*	3.64	1.73	19.32	9.37	0.70	7.79	3.78
0.875	0	0.125	10.4747(32)	−7.1	–	*1.76*	2.28	0.48	17.69	14.87	0.19	7.14	6.00
0	0.125	0.875	10.4553(28)	4.7	1023	3.20	3.28	23.80	22.10	0.59	9.60	8.91	0.24
0	0.25	0.75	10.4324(8)	6.6	1098	5.13	5.41	34.41	14.99	2.22	13.88	6.05	0.90
0	0.375	0.625	10.4154(6)	10.4	1148	6.31	6.50	42.53	9.54	4.68	17.16	3.85	1.89
0	0.5	0.5	10.3602(9)	1.9	1173	6.76	6.66	47.73	5.55	7.77	19.26	2.24	3.14
0	0.625	0.375	10.2650(24)	−19.2	1173	6.45	5.98	49.60	2.81	11.27	20.01	1.13	4.55
0	0.75	0.25	10.2559(14)	−12.7	1123	5.25	4.58	47.73	1.11	14.99	19.26	0.45	6.05
0	0.875	0.125	10.2116(33)	−17.3	1048	3.28	2.55	41.69	0.24	18.70	16.82	0.10	7.55
0.5	0.25	0.25	10.4512(14)	7.6	1073	9.28	8.43	1.08	18.28	13.29	0.43	7.37	5.36
0.25	0.5	0.25	10.3452(20)	−5.5	1198	10.36	10.49	11.43	7.23	16.08	4.61	2.92	6.49
0.25	0.25	0.5	10.4517(15)	10.3	1098	9.49	9.70	8.86	20.31	4.80	3.58	8.19	1.94
0.333	0.333	0.333	10.4260(13)	8.4	1123	10.26	10.44	5.02	15.21	11.10	2.02	6.14	4.48

Data obtained by extrapolation of experimental data was signed by italic type.

of minimal temperature, i.e. the temperature at which the sample was found out to be monophasic, as the mixing temperature (see Table 1).

In order to decrease the kinetic factor connected in general with diffusion processes, in every synthesis step the samples were dispersed using the vibration grinding mill Mixer/Mill5100. This treatment led to increase of the surface area of interacting particles. Then the powders were pressed at 100 bar. After determining the mixing temperatures the samples were calcined at 1273 K to increase their crystallinity.

As can be seen in Table 1 the mixing temperatures for $KNbWO_6$–$KTaWO_6$ system are not defined since their values are lower than synthesis temperatures of these solid solutions. Therefore, formation of monophase sample was observed already at 973 K. It is worth to notice that the obtained solid solutions are stabilized with respect to unmixing process at room temperature.

2.2. Apparatus and measurement procedure

For structural investigations, X-ray diffraction patterns of all samples were recorded on a Shimadzu X-ray diffractometer XRD-6000 (Cu Kα radiation, geometry θ–2θ) in the 2θ range from 10° to 120° with scan increment of 0.02°. Rietveld analysis and structure refinement [8] were carried out using RIETAN-94 software [9].

Polycrystalline infrared spectra were measured with a Biorad 575C FT-IR spectrometer in KBr suspension for the 1000–400 cm^{-1} region and in Nujol suspension for the 500–40 cm^{-1} region. FT-Raman spectra were measured using BRUKER 110/S spectrometer. Excitation was performed with a 1064 nm line of a YAG:Nd^{3+} laser. Both IR and Raman spectra were recorded with a spectral resolution of 2 cm^{-1}.

Thermal behavior was carried out with DSC Labsys from Setaram in a platinum crucible ranging from 293 to 1173 K (heating rate 0.167 K/s).

3. Results and discussion

3.1. Crystal structure

Structure of individual compounds ($KNbWO_6$, $KSbWO_6$ and $KTaWO_6$) was refined by the Rietveld method, assuming space group $Fd\bar{3}m$ and having defect pyrochlore structure. The initial model included the atomic coordinates in the structure of $RbNbWO_6$ [10]. The details of the X-ray diffraction experiment and structure refinement data are listed in Table 2. Fig. 1 represents the measured, simulated, and difference X-ray diffraction patterns for $KNbWO_6$, as well as a pattern of lines corresponding to reflection maxima. There is a good agreement between the measured and simulated patterns. Table 3 lists the coordinates of the atoms and their isotropic thermal parameters. The refined model yielded positive isotropic thermal parameters B for all atoms. Table 4 lists the interatomic distances and valence angles in the structure and Fig. 2

Table 2
Details of the X-ray diffraction experiment and the results of the structure refinement for KA^VWO_6 (A^V – Nb, Sb, Ta) (all data presented at T = 298 K).

	$KNbWO_6$	$KSbWO_6$	$KTaWO_6$
Space group	$Fd\bar{3}m$		
Z	8		
2θ range (°)	10–120		
a (Å)	10.5001(1)	10.23671(7)	10.4695(1)
V (Å^3)	1157.67(2)	1072.71(1)	1147.57(3)
d (kg m^{-3})	4752.9	5488.6	5819.7
'Number of reflections	59	63	55
Number of refined parameters	25	27	27
Structural parameters	4	6	4
Others	21	21	23
R_{wp}; R_p (%)	8.53; 5.40	3.75; 2.63	10.11; 6.48

Definition of reliability factors R_{wp} and R_p are given as follows: $R_{wp} = \{(\sum w_i[y_{iobs} - y_{icalc}]^2/(\sum w_i[y_{iobs}]^2)\}^{1/2}$; $R_p = (\sum |y_{iobs} - y_{icalc}|)/(\sum y_{iobs})$.

Table 3
Coordinates and isotropic thermal parameters of atoms in the structure of $KA^{V}WO_6$ (A^{V} – Nb, Sb, Ta).

Atom	Site	*x*	*y*	*z*	Occ	*B* (Å²)
$KNbWO_6$						
K	32e	0.4845(5)	0.4845(5)	0.4845(5)	0.25	1.08(3)
Nb	16c	0	0	0	0.5	1.08(3)
W	16c	0	0	0	0.5	1.08(3)
O	48f	0.3211(5)	0.125	0.125		1.08(3)
$KSbWO_6$						
K	32e	0.4010(5)	0.4010(5)	0.4010(5)	0.25	2.0(3)
Sb	16c	0	0	0	0.5	0.85(2)
W	16c	0	0	0	0.5	0.85(2)
O	48f	0.3206(3)	0.125	0.125		0.9(1)
$KTaWO_6$						
K	32e	0.4851(7)	0.4851(7)	0.4851(7)	0.25	0.95(3)
Ta	16c	0	0	0	0.5	0.95(3)
W	16c	0	0	0	0.5	0.95(3)
O	48f	0.3151(7)	0.125	0.125		0.95(3)

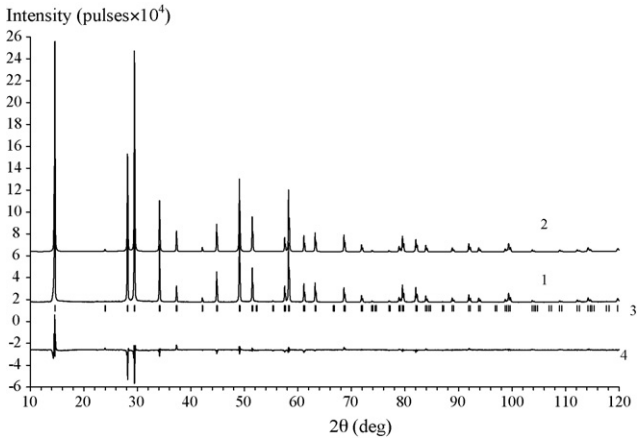

Fig. 1. Fragments of (1) observed, (2) simulated, and (4) difference X-ray diffraction patterns for $KNbWO_6$, and (3) Bragg reflections. The simulated pattern is shifted relative to the observed pattern.

represents a fragment of the $KNbWO_6$ structure. The $(Nb/W)O_6$ octahedra share corners to form a three-dimensional framework possessing tunnels running down the *c*-axis in which the potassium cations are located. The Nb/W cation is located in the 16c Wyckoff position (0, 0, 0) and the oxygen is in 48f sites (*x*, 1/8, 1/8). The location of the potassium is in the 32e site (*x*, *x*, *x*). It should be noted that location of the potassium is the same in the three compounds independently of framework composition. Therefore investigated individual compounds are isostructural.

Table 4
Interatomic distances and valence angles in the structure of $KA^{V}WO_6$ (A^{V} – Nb, Sb, Ta).

Bond	*d* (Å)	Angle	*ω* (°)
$KNbWO_6$			
Nb/W–O (×6)	2.001(2)	O–Nb/W–O (×3)	93.4
K–O (×3)	2.609(4)	O–Nb/W–O (×3)	86.6
K–O (×3)	2.701(4)		
$KSbWO_6$			
Sb/W–O (×6)	1.949(1)	O–Sb/W–O (×3)	86.8
K–O (×3)	2.874(5)	O–Sb/W–O (×3)	93.2
K–O (×3)	3.346(5)		
$KTaWO_6$			
Ta/W–O (×6)	1.972(2)	O–Ta/W–O (×3)	89.0
K–O (×3)	2.652(4)	O–Ta/W–O (×3)	91.0
K–O (×3)	2.731(4)		

The unit cell parameters of the compounds and solid solutions were calculated using the analytical indexing technique (Table 1). All compounds were indexed in terms of the cubic crystal system and have defect pyrochlore structure.

Analysis of the X-ray diffraction data shows that the $KNb_xSb_yTa_zWO_6$ ternary system is characterized by complete solid miscibility at $T > 1198$ K and that the unit cell volumes obey the Retgers rule [11], with insignificant deviations (<1.8%). There is negative variance from Retgers rule for $KNb_xSb_yTa_zWO_6$ solid solutions where $y > 0.5$ (Fig. 3), that confirms more strong chemical bonds in the solid solution in comparison with individual compounds.

3.2. Raman and IR

According to the structural data, the primitive unit cell of the studied pyrochlores consists of two formula units. The oxygen (48f site), M/W, where M = Nb, Ta or Sb (16c site) and potassium (32e site) contribute with $A_{2u} + E_u + 2F_{2u} + 3F_{1u} + A_{1g} + E_g + 3F_{2g} + 2F_{1g}$, $A_{2u} + E_u + F_{2u} + 2F_{1u}$ and $A_{2u} + E_u + F_{2u} + 2F_{1u} + A_{1g} + E_g + 2F_{2g} + F_{1g}$ modes, respectively. The A_{1g}, F_{2g} and E_g mode are Raman-active and the F_{1u} modes are IR-active. It should be noticed, however, that one of the F_{1u} modes corresponds to the acoustic mode. Therefore, one expects to observe 9 Raman-active ($2A_{1g} + 2E_g + 5F_{2g}$) and 6 IR-active F_{1u} optical modes.

The IR and Raman spectra are presented in Figs. 4 and 5. The former studies of $A_2B_2O_7$ pyrochlores, where A = Y, Gd, Dy, In, Tl and B = Ru, Mn, Ti, showed that the highest wavenumber IR band can be

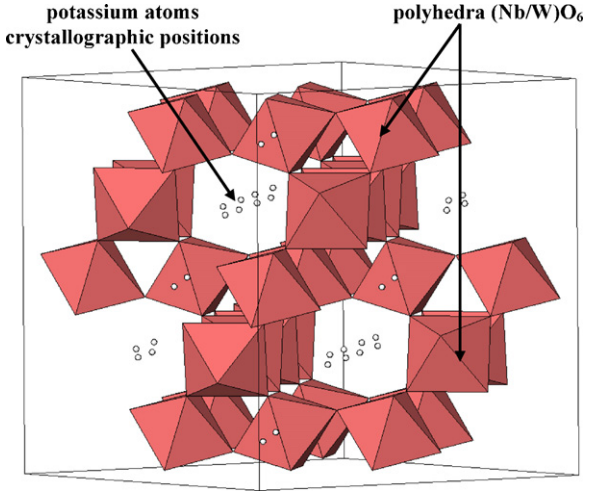

Fig. 2. Fragment of the structure of $KNbWO_6$.

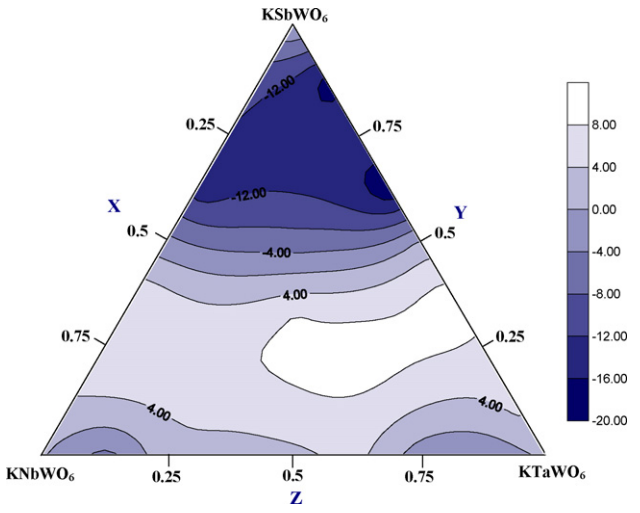

Fig. 3. Projections of the volume of mixing surface for the $KNbWO_6$–$KSbWO_6$–$KTaWO_6$ system (definition of $\Delta_{mix}V$ is given as follow: $\Delta_{mix}V = V(KNb_xSb_yTa_zWO_6) - (x \cdot V(KNbWO_6) + y \cdot V(KSbWO_6) + z \cdot V(KTaWO_6))$).

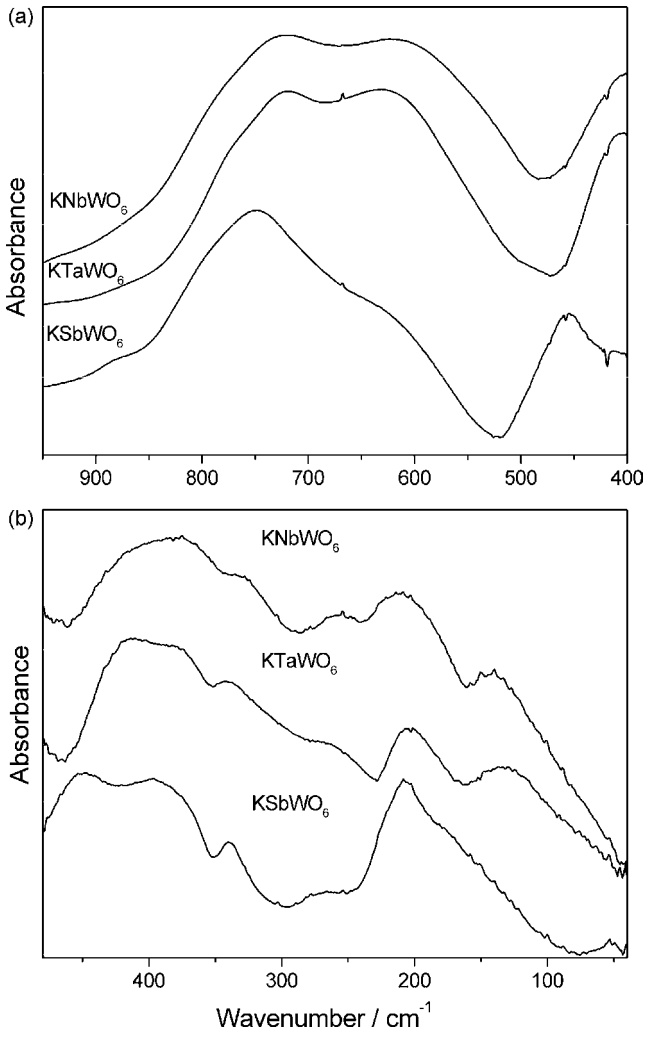

Fig. 4. Mid- (a) and far-IR (b) spectra of $KNbWO_6$, $KTaWO_6$ and $KSbWO_6$.

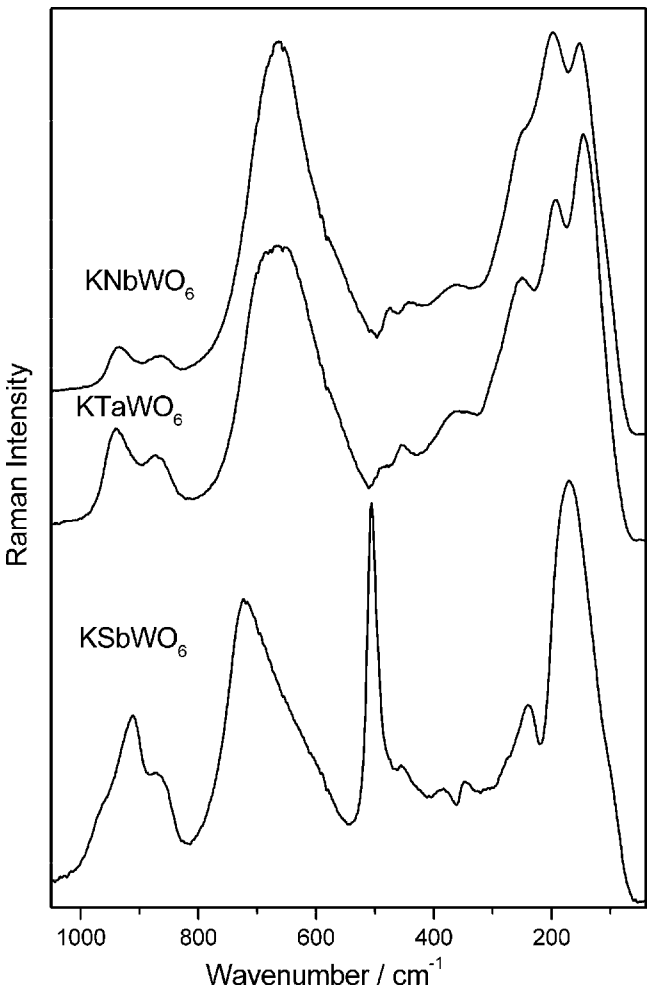

Fig. 5. Raman spectra of $KNbWO_6$, $KTaWO_6$ and $KSbWO_6$.

assigned to stretching mode of the BO_6 octahedra. This band was observed in the range 542–595 cm^{-1}. The bending modes of the BO_6 octahedra were observed in the range 200–500 cm^{-1}[12–15]. Our IR spectra of $KNbWO_6$, $KTaWO_6$ and $KSbWO_6$ reveal presence of two strong and broad bands in the mid-IR region near 719–748 and 618–635 cm^{-1}. We assign these bands to the stretching modes of the M/WO_6 octahedra (M = Nb, Ta or Sb). As can be noticed, these modes are observed at significantly higher wavenumbers than the stretching modes of the titanium, manganese or rutenium pyrochlores. This result can be attributed to higher valence state of the M/W atoms, in comparison with the Ti or Ru atoms, and significant differences of the structural arrangement between the $A_2B_2O_7$ pyrochlores and $KNbWO_6$, $KTaWO_6$ and $KSbWO_6$ defect pyrochlores. In particular, the oxygen atoms in the M/WO_6 octahedra are connected to the potassium atoms, instead of trivalent atoms in the titanium or rutenium pyrochlores, and one oxygen sublattice (8a site in the $A_2B_2O_7$ pyrochlores) is empty. The IR spectra show also presence of weak bands in the range 878-935 cm^{-1}. These bands can be most likely assigned to stretching modes of the terminal –M/W=O bonds, which appear due to some structural defects. In the bending and lattice modes region, i.e. below 500 cm^{-1}, six bands are observed (see Table 5). Translational motions of the M/W atoms contribute most likely only to the lowest wavenumber band since for $KTaWO_6$ and $KNbWO_6$ this band exhibits shift towards higher wavenumbers with decreasing atomic mass, i.e. it is observed at 133 and 142 cm^{-1}, respectively. For $KSbWO_6$ this band is observed at 163 cm^{-1}, although the atomic

Table 5
Raman and IR wavenumbers for $KNbWO_6$, $KTaWO_6$ and $KSbWO_6$ together with the proposed assignment. *T* denotes translational modes. S, m, w, sh and b denote strong, medium, weak, shoulder and broad, respectively.

$KNbWO_6$		$KTaWO_6$		$KSbWO_6$		Assignment
IR	Raman	IR	Raman	IR	Raman	
–	–	–	–	–	960sh	
935w	934w	933w	937w	–	909m	Stretching modes of the terminal –M/W=O bonds
–	861w	–	870w	874w	864w	
719s	664s	719s	664s	748s	721s	
618s	576m,b	629s	580m,b	635m	654s,b	Stretching modes of M/WO_6
–	473w	–	481w	–	506s	
408s	–	412s	–	449m	–	
385s	438w	382m	452w	395m	453w	Bending modes of M/WO_6
329w	360w	340m	359w	340w	382w	
255w		263sh		267w	343w	
212m	246sh	203m	248m	208m	239w	Bending modes of M/WO_6 coupled with *T* (K)
–	196s	–	191s	–	169s	
–	152s	–	145s	–	–	*T* (M/W)
142w		133m		163m,b		

mass of Sb is higher than the atomic mass of Nb. This result can be attributed to the fact that the Sb atoms are more tightly bound in the structure than Nb atoms (see discussion below). The IR spectra show also two interesting features. First, the number of the observed bands is larger (8) than predicted by the factor group analysis (6). The appearance of more than six IR modes can be attributed to the partial breakdown in selection rules due to the partial occupancy of the 32 site (0.25) and positional disorder at the 16c site. As a result, some silent or Raman-active modes may appear in the IR spectra. Second, the spectra of $KTaWO_6$ and $KNbWO_6$ are very similar each to other whereas the spectra of $KSbWO_6$ show large changes in relative intensities of bands and strong shifts of a few bands towards higher waveumbers. This behavior can be attributed to much smaller size of the Sb(V) in comparison with Nb(V) and Ta(V) atoms. As a result the Sb/W atoms are more tightly bound to oxygens than the Nb/W or Ta/W atoms and, consequently, some bands exhibit significant shifts towards higher wavenumbers due to shortening of the M/W–O bonds.

Raman spectra of $A_2B_2O_7$ pyrochlores (A = Y, Gd, Dy, In, Tl and B = Ru, Mn, Ti, Zr) have been the subject of numerous studies [12–19]. These studies showed that the A_{1g} mode gives rise to strong Raman band, which is observed near 489–543 cm^{-1} [12–19]. Two other strong bands were observed in the 289–318 and 327–350 cm^{-1} regions, and assigned to F_{2g} and E_g modes, respectively [12–19]. The remaining F_{2g} modes were usually weak and observed in the 180–245, 390–460, 510–600 cm^{-1} regions [12–19]. For molybdenum pyrochlore, $Nd_2Mo_2O_7$, only three strong A_{1g}, E_g and F_{2g} bands were observed at significantly lower wavenumbers, i.e. 488, 294 and 265 cm^{-1}, respectively [20]. Recent studies of defect pyrochlore KOs_2O_6 showed that its spectrum is very similar to the spectra of $A_2B_2O_7$ pyrochlores but the bands are shifted towards lower wavenumbers [21]. The most intense A_{1g} and F_{2g} modes were observed at 490 and 237 cm^{-1}, respectively, and the E_g mode was observed as a weak band at 262 cm^{-1} [21]. The three remaining F_{2g} modes were observed at 705 and 72 cm^{-1} and calculated at 426 cm^{-1}. The mode near 72 cm^{-1} was assigned to translations of the potassium ions [21]. Our Raman spectra of $KTaWO_6$, $KNbWO_6$ and $KSbWO_6$ differ very much from the Raman spectra of $A_2B_2O_7$ and KOs_2O_6 pyrochlores. First, there are a few bands in the 860–960 cm^{-1} region, which can be attributed to stretching modes of the –M/W=O terminal bonds. Such bands are not present for the $A_2B_2O_7$ pyrochlores. Second, a very intense band is observed near 660–720 cm^{-1} whereas for the $A_2B_2O_7$ and KOs_2O_6 pyrochlores no strong bands were observed above 550 cm^{-1}. This band is very broad and asymmetric, and therefore it is composed of at least two components (see Table 5). We assign this band to the F_{2g} stretching mode of the M/WO_6 octahedra and the presence of two components can be attributed to the positional disorder, as discussed above for the IR spectra. Third, a strong and relatively narrow band is observed for $KSbWO_6$ at 506 cm^{-1}. In analogy with the other pyrochlores mentioned above, this band can be most likely assigned to the A_{1g} mode. It is interesting to notice that for $KTaWO_6$ and $KNbWO_6$ the A_{1g} bands are weak. Fourth, in contrast to the $A_2B_2O_7$ and KOs_2O_6 pyrochlores, which showed only weak Raman bands below 200 cm^{-1}, very intense bands are observed in this range for $KTaWO_6$, $KNbWO_6$ and $KSbWO_6$. These bands can be assigned to bending modes of the M/WO_6 octahedra coupled with translational modes of the potassium ions.

3.3. A physicochemical subregular ternary solutions model

When studying isomorphism, one needs to know not only the type of solid solution and the miscibility regions but also the energy parameters of this phenomenon. Provided that the thermodynamic functions of mixing are known, one can answer many questions concerning the character of the solid solution formation and the thermodynamic stability regions of the solutions. We will consider the behavior of the thermodynamic functions of mixing in ternary systems using the title system as an example.

We used the mixing temperatures for all compositions in order to calculate the standard enthalpy of mixing (Table 1), basing on formula: $\Delta_{mix}H^\circ = T_{mix} \cdot \Delta_{mix}S^\circ$, where $\Delta_{mix}S^\circ = \Delta_{conf}S^\circ + \Delta_{vibr}S^\circ$. But according to Ref. [23] $\Delta_{vibr}S^\circ$ could possess the sizable value only when $\Delta R/R > 0.1$ (where R – ionic radii of the substitute atoms). Whereas, in our case $\Delta R/R \leq 0.06$ and corresponding value of $\Delta_{vibr}S^\circ$ is equal to 0.25 J mol^{-1} K^{-1} [23], so, we can neglect this item. The possible error of this assumption is no more than 8%.

Thus, $\Delta_{mix}S^\circ$ is taken as configuration entropy and calculated according the equation: $\Delta_{mix}S^\circ = -R \cdot (x \cdot \ln x + y \cdot \ln y + z \cdot \ln z)$, where R = 8.314 J mol^{-1} K^{-1}, x, y and z – mole percent of Nb, Sb and Ta correspondingly. Error connected with 25 K temperature step in the experiments is no more than two percent, so summing all above-mentioned it could be possible to conclude that error of calculated enthalpies of mixing is no more than ten percent that could be compared with calorimetric measurements.

Mixing in all cases is endothermic, and the enthalpies of mixing do not exceed 10.5 kJ mol^{-1} (Table 1). The highest enthalpy of mixing refers to the composition $KNb_{0.25}Sb_{0.75}Ta_{0.25}WO_6$.

A subregular model can describe the derived composition dependence of the enthalpy of mixing mapped as a surface (Fig. 6).

The regular model, theoretically developed by Prigozhin and Defay [22], is inapplicable for the system in question: in terms of this model, the enthalpy of mixing surface should have a maximum near one of the binary systems, which does not occur in our case. Therefore, we advanced a theoretical subregular solutions model for ternary systems. This model allows us to show changes in the thermodynamic functions in the form of analytical equations, simplifying the quantitative representation of systems and giving the partial molar quantities and the activity coefficients for the components. In terms of this model, the maximal value of the enthalpy of mixing is observed for random concentrations of the three components. Therefore, the enthalpy of mixing should be presented as a function of composition in the form of four summands. Three summands describe the behavior of the function near binary systems, and the fourth summand, in the central portion of the diagram. Based on this, the equation for the enthalpy of mixing reads:

$$\Delta_{mix}H = k[X\cdot Y\cdot(X+a_1\cdot Y)+X\cdot Z\cdot(X+a_2Z) + Y\cdot Z\cdot(Y+a_3Z)+X\cdot Y\cdot Z\cdot(X+a_4Y+a_5Z)] \quad (1)$$

where k is a constant factor and a_i are factors showing the subregularity of the system.

Eq. (1), which describes the subregular solutions model for ternary systems, is transformed, when the third component concentration is null ($z=0$), to the equation derived in [23] to describe subregular solutions for binary systems. Provided that the a_i values are equal to unity, Eq. (1) is transformed to the regular solutions equation for ternary systems [22].

We used relationships between the integral and partial molar quantities known from thermodynamics [23], to derive equations for the partial molar enthalpies of mixing in which the polynomial factors b_i, c_i, and d_i are expressed through the a_i factors (Table 6).

Once we knew the partial molar enthalpies of mixing, we calculated the activity coefficients for the components of the solid solution (Eq. (3), Table 1). The activity coefficients allow us to judge the interaction character between the components in a solid.

$$\Delta_{mix}H = X\cdot\Delta\bar{H}_1 + Y\cdot\Delta\bar{H}_2 + Z\cdot\Delta\bar{H}_3 \quad (2)$$

$$\begin{cases} \Delta\bar{H}_1 = \Delta_{mix}H - Y\dfrac{\partial\Delta_{mix}H}{\partial Y} - Z\dfrac{\partial\Delta_{mix}H}{\partial Z} = RT\ln\gamma_1 \\ \Delta\bar{H}_2 = \Delta_{mix}H - X\dfrac{\partial\Delta_{mix}H}{\partial X} - Z\dfrac{\partial\Delta_{mix}H}{\partial Z} = RT\ln\gamma_2 \\ \Delta\bar{H}_3 = \Delta_{mix}H - X\dfrac{\partial\Delta_{mix}H}{\partial X} - Y\dfrac{\partial\Delta_{mix}H}{\partial Y} = RT\ln\gamma_3 \end{cases} \quad (3)$$

$$\begin{cases} \Delta\bar{H}_1 = k[b_1Y^2 + b_2Y\cdot Z + b_3Y^3 + b_4Y^2\cdot Z + b_5Z^2\cdot Y + b_6Z^2 + b_7Z^3 + b_8Y^3\cdot Z + b_9Y^2\cdot Z^2 + b_{10}Z^3\cdot Y] \\ \Delta\bar{H}_2 = k[c_1X^2 + c_2X\cdot Z + c_3X^3 + c_4X^2\cdot Z + c_5Z^2\cdot X + c_6Z^2 + c_7Z^3 + c_8X^3\cdot Z + c_9X^2\cdot Z^2 + c_{10}Z^3\cdot X] \\ \Delta\bar{H}_3 = k[d_1X^2 + d_2X\cdot Y + d_3X^3 + d_4X^2\cdot Y + d_5Y^2\cdot X + d_6Y^2 + d_7Y^3 + d_8X^3\cdot Y + d_9X^2\cdot Y^2 + d_{10}Z^3\cdot X] \end{cases} \quad (4)$$

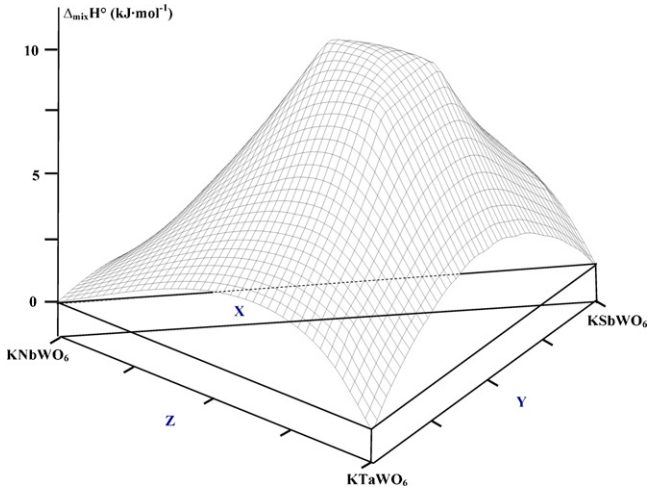

Fig. 6. Enthalpy of mixing vs. composition for $KNb_xSb_yTa_zWO_6$.

The mathematical model fits the experiment well when applied to the system under study. The optimal a_i and k values were found, using consecutive approximations, for Eq. (1) to fit the experimentally derived surface well. In the description of the enthalpy of mixing as a function of composition for $KNb_xSb_yTa_zWO_6$, the factors in Eq. (1) have the following values: $k=22.2$, $a_1=1.4$, $a_2=0.5$, $a_3=1.4$, $a_4=9.5$, and $a_5=8.7$.

Fig. 7 shows the projections of the experimentally derived and theoretical enthalpy of mixing surfaces on the triangular diagram in the form of equal level line maps.

The examination of the maps enables us to state that the energy factor contributes more to the enthalpy of mixing, which may be due to the difference between the electronegativities of the substitute atoms; the dimensional factor is less probable here, since the ionic radii of the substitute atoms are very close to each other. The key role of the energy factor was deduced from the fact that the maximum of the enthalpy of mixing surface is displaced to the compositions richer in antimony; this displacement may be associated with the antimony atom having a higher electronegativity (equal to 2.05 on Pauling's scale [11]) against the values of 1.60 and 1.50 for the niobium and tantalum atoms, respectively.

It is important to draw attention that similar influence of the difference between the electronegativities of the substitute atoms on the pattern of mixing was investigated on the $Mg_{0.33}Mn_{0.33}Co_{0.33}UO_2(SO_4)_2\cdot5H_2O$ system and described earlier by Chernorukov et al. [24].

3.4. Differential scanning calorimetry

Joint application of the high temperature X-ray diffraction and thermal analysis (TG–DTA) made it possible to establish some

Table 6
Factors in polynomials (4).

	b	c	d
1	$2-a_1$	$2a_1-1$	$2a_2-1$
2	3	$2a_1-a_4+2$	$2a_2+2a_3-a_5$
3	$2a_1-2$	$2-2a_1$	$2-2a_2$
4	$2a_1-2a_4-4$	$4a_4-4a_1-4$	$4a_5-2a_3-4a_2-2$
5	$2a_2-2a_5-2a_3-2$	$4a_4+2a_3-2a_1-2a_2-2a_5-4$	$4a_5-2a_4-4a_3-2a_2-2a_1+2$
6	$2-a_2$	$2-a_3$	$2a_3-1$
7	$2a_2-2$	$2a_3-2$	$2-2a_3$
8	$3a_4-3$	$3-3a_4$	$3-3a_5$
9	$3a_4+3a_5-6$	$3a_5-6a_4+3$	$3a_4-6a_5+3$
10	$3a_5-3$	$3a_5-3a_4$	$3a_4-3a_5$

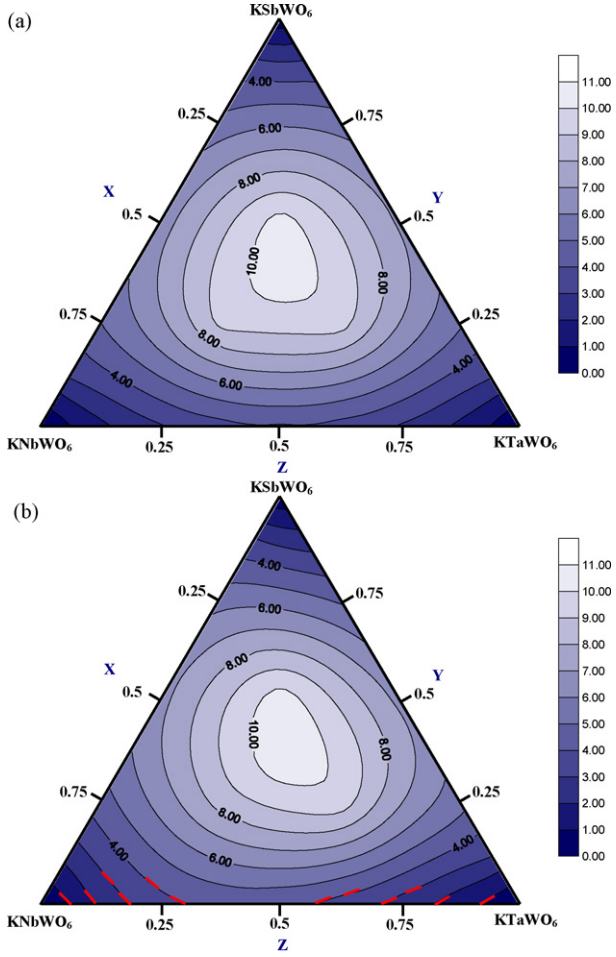

Fig. 7. Calculated(a) and experimentally derived (b) projections of the enthalpy of mixing surfaces for $KNbWO_6$–$KSbWO_6$–$KTaWO_6$ system (data obtained by extrapolation of experimental data was signed by red dotted line). (For interpretation of the references to color in this figure legend, the reader is referred to the web version of the article.)

peculiarities of processes taking place in the compounds under investigation during heating. Fig. 8 represents DTA curves of individual compounds of the titled system, where we can see endothermic effects at 1323 K for $KNbWO_6$, 1446 K for $KTaWO_6$, and two endothermic effects at 1302K and 1361K for $KSbWO_6$. It was not observed any mass changes on TG curve during experiment, so we can draw a conclusion that the stoichiometric composition of systems did not change. The first effect for $KSbWO_6$ is connected with irreversible polymorphic transition, which can be confirmed by X-ray diffraction data according to Ref. [25]. The second effect for $KSbWO_6$ and effects on DTA curve of $KNbWO_6$ and $KTaWO_6$ are connected with incongruent melting of $KSbWO_6$ and $KNbWO_6$ and the solid phase thermal decomposition in $KTaWO_6$. After these effects parent phases were not detected. Melting products, found out by XRD analysis, were not identified due to complexity of their compositions and lack in PDF 4 and FindIt XRD databases, whereas the products of the solid phase thermal decomposition in $KTaWO_6$ were recognized, thus thermal decomposition may be represented by the following scheme:

$$KTaWO_6(cr) \rightarrow 5/7K_{1.4}Ta_{1.4}W_{0.6}O_6(cr) + 4/7WO_3(cr)$$

It can be seen that the studied compounds have high thermal stability.

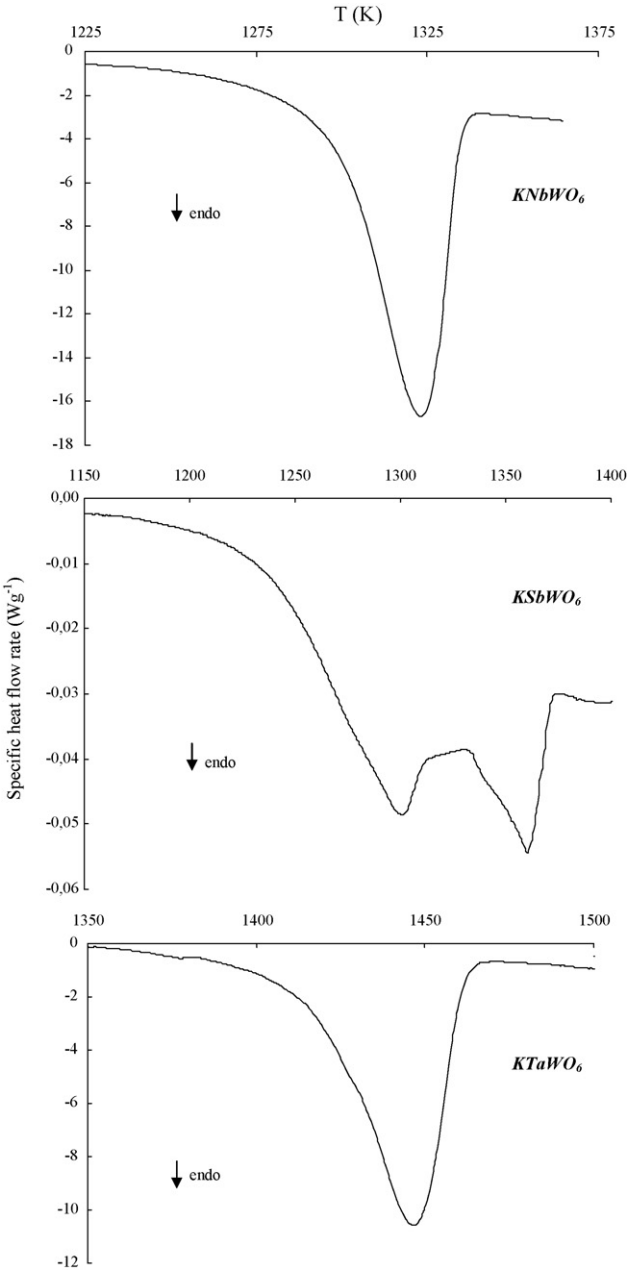

Fig. 8. Plot of the DTA-signal against temperature for KA^VWO_6 (A^V – Nb, Sb, Ta).

4. Conclusions

To conclude, we were the first to synthesize and characterize solid solutions with the composition $KNb_xSb_yTa_zWO_6$. The mathematical model advanced for ternary subregular solid solutions has a predictive power. Our results highlight certain tendencies for the energy factor to dominate over the dimensional factor in the study of isomorphism in the title system. Also we used X-ray diffraction data and IR and Raman spectroscopy for determination of structural pecularities. Besides it was shown by the differential scanning calorimetry that these compounds have high thermal stability and either melt incongruently or decompose thermally in the solid phase.

References

[1] T. Kar, R.N.P. Choudhary, J. Phys. Chem. Solids 62 (2001) 1149.

[2] J.A. Diaz-Guillen, M.R. Diaz-Guillen, K.P. Padmasree, A.F. Fuentes, J. Santamaria, C. Leon, Solid State Ionics 179 (2008) 2160.
[3] B.C. Chakoumakos, J. Solid State Chem. 53 (1984) 120.
[4] R.M. McCauley, J. Appl. Phys. 51 (1980) 290.
[5] M.A. Subramanian, G. Aravamudan, G.V. SubbaRao, Progr. Solid State Chem. 15 (1983) 55.
[6] J.E. Greedan, J. Alloys Compd. 408–412 (2006) 444–455.
[7] T. Kar, R.N.P. Choudhary, J. Solid State Chem. 141 (1998) 50.
[8] H.M. Rietveld, Acta Crystallogr. 22 (Part 1) (1967) 151.
[9] F. Izumi, Rietveld analysis programs RIETAN and PREMOS and special applications, in: R.A. Young (Ed.), The Rietveld Method, Oxford University Press, Oxford, 1993, p. 236.
[10] N.N. Bydanov, T.S. Chernaya, L.A. Muradyan, V.A. Sarin, E.E. Rider, V.K. Anovskii, A.A. Bosenko, Kristallografiya 32 (1987) 623.
[11] V.S. Urusov, Theoretical Crystal Chemistry, Izd. Mosk. Gos. Univ., Moscow, 1987, p. 275 (in Russian).
[12] H.C. Gupta, N. Rani, J. Phys. Chem. Solids 68 (2007) 1293.
[13] S. Brown, H.C. Gupta, J.A. Alonso, M.J. Martinez-Lope, Phys. Rev. B 69 (2004) 054434.
[14] A.F. Fuentes, K. Boulahya, M. Maczka, J. Hanuza, U. Amador, Solid State Sci. 7 (2005) 343.
[15] H.C. Gupta, S. Brown, N. Rani, V.B. Gohel, J. Raman Spectrosc. 32 (2001) 41.
[16] N.J. Hess, B.D. Begg, S.D. Conradson, D.E. McCready, P.L. Gassman, W.J. Weber, J. Phys. Chem. B 106 (2002) 4663.
[17] M. Maczka, J. Hanuza, K. Hermanowicz, A.F. Fuentes, K. Matsuhira, Z. Hiroi, J. Raman Spectrosc. 39 (2008) 537.
[18] M. Maczka, M.L. Sanjuán, A.F. Fuentes, K. Hermanowicz, J. Hanuza, Phys. Rev. B 78 (2008) 134420.
[19] M. Maczka, M.L. Sanjuán, A.F. Fuentes, L. Macalik, J. Hanuza, K. Matsuhira, Z. Hiroi, Phys. Rev. B 79 (2009) 214437.
[20] K. Taniguchi, T. Katsufuji, S. Iguchi, Y. Taguchi, H. Takagi, Y. Tokura, Phys. Rev. B 70 (2004) 100401R.
[21] T. Hasegawa, Y. Takasu, N. Ogita, M. Udagawa, Phys. Rev. B 77 (2008) 064303.
[22] I. Prigogin, R. Defay, Chemical Thermodynamics, Longmans Green, London, 1954, Nauka, Moscow, 1966.
[23] V.S. Urusov, Theory of Isomorphous Miscibility, Nauka, Moscow, 1977 (in Russian).
[24] N.G. Chernorukov, A.V. Knyazev, R.A. Vlasov, Yu.S. Sazhina, Russ. J. Inorg. Chem. 49 (2004) 978.
[25] A.V. Knyazev, I.G. Tananaev, N.Yu. Kuznetsova, N.N. Smirnova, I.A. Letyanina, I.V. Ladenkov, Thermochim. Acta 499 (2010) 155.